



Effect of heat treatments on microstructure/small-scale properties of additive manufactured Ti-6Al-4V

Muztahid Muhammad¹ · Jonathan W. Pegues^{2,3} · Nima Shamsaei^{2,3} · Meysam Haghshenas¹

Received: 31 January 2019 / Accepted: 16 April 2019 / Published online: 19 May 2019
© Springer-Verlag London Ltd., part of Springer Nature 2019

Abstract

In the present study, the effect of various heat treatments on the microstructure and micromechanical properties of a Ti-6Al-4V alloy processed by a laser powder bed fusion (L-PBF) technique is investigated. Heat treatment cycles employed in this study include solutionizing at 950 °C (for 1 h) followed by three different cooling rates (water quenching, air cooling, and furnace cooling) as well as solutionizing followed by water quenching and artificial aging. To assess the small-scale properties, a nanoindentation testing technique is employed. Microstructural quantitative analyses (i.e., optical microscopy and scanning electron microscopy) were performed extensively on the as-fabricated and heat-treated samples. Artificially aged specimens showed the highest microhardness of all the heat-treated samples, followed by air-cooled and furnace-cooled samples.

Keywords Ti-6Al-4V · Additive manufacturing · Heat treatment · Nanoindentation · Artificial aging

Nomenclature

A	Indentation area
C	Sink-in/pile-up factor
E	Modulus of the specimen
E_i	Modulus of the indenter
H_{ind}	Indentation hardness
h	Indentation displacement
h_c	Instantaneous contact depth
h_{max}	Maximum indentation depth
P_{ind}	Indentation load
R	Indenter tip radius due to blunting at tip
α	Hexagonal close packed (HCP) Ti
α'	Supersaturated α in β stabilizing elements
α''	Orthorhombic α
β	Body-centered cubic Ti
σ_{ind}	Indentation stress
ν	Poisson's ratio of the specimen

ν_i Poisson's ratio of the indenter

1 Introduction

Due to both inherent costly raw materials and difficulties associated with its conventional manufacturing (i.e., welding and machining), Ti-6Al-4V alloy is naturally suited to additive manufacturing (AM). In addition, additive manufactured Ti-6Al-4V offers decreased labor cost and material waste, less processing, smaller footprints, shorten manufacturing time, and most significantly, tailored properties in the finished component. The AM processes, however, exhibit a quite different cooling rate and thermal gradient in comparison to the conventional manufacturing methods [1]. Despite providing numerous benefits, the AM Ti-6Al-4V experiences undesirable microstructures consisting of large columnar prior β grains across the entire height of the builds which lead to anisotropy [2, 3].

Laser powder bed fusion (L-PBF) is a suitable and well-developed AM technique to fabricate Ti-6Al-4V alloys. The L-PBF technique, which is also known as direct metal laser sintering (DMLS), uses high power density laser to melt and fuse metallic powder together [4]. Due to the specific microstructure originating from the L-PBF process [5], specific treatments are required to obtain optimal mechanical properties. The microstructure of Ti-6Al-4V alloy manufactured by

✉ Meysam Haghshenas
meysam.haghshenas@engr.und.edu

¹ Department of Mechanical Engineering, University of North Dakota, Grand Forks, ND 58202, USA

² Department of Mechanical Engineering, Auburn University, Auburn, AL 36849, USA

³ National Center for Additive Manufacturing Excellence (NCAME), Auburn University, Auburn, AL 36849, USA

the L-PBF process typically consists of a fine acicular martensite known as the α' phase [6, 7]. Although these L-PBF Ti-6Al-4V parts typically exhibit a high ultimate tensile strength, and a high yield stress (about 1 GPa), they have a relatively low ductility (less than 10%) [8]. To obtain a variety of desired mechanical properties for specific applications along with improvement in the ductility of Ti-6Al-4V alloy parts manufactured by the L-PBF, appropriate post-production heat treatment processes must be elaborated. Moreover, these heat treatments cause the reduction of thermal stresses built up during the additive manufacturing processes and further assist with enhancing the part performance.

The effect of post-fabrication heat treatment on microstructure and micromechanical properties of conventionally fabricated Ti alloys has been reported in numerous studies [9–12]. In general, through heat treatment of conventionally manufactured Ti-6Al-4V alloy, the hardness increases as the rate of cooling increases due to the formation of martensite arising from rapid cooling [13–15]. Although there are numerous data on the conventionally manufactured Ti-6Al-4V alloy, limited studies involving the effect of microstructure and micromechanical characteristics of the AM Ti-6Al-4V alloy have been reported in the literature till date [16].

Wrought Ti-6Al-4V is generally supplied in the mill-annealed condition after the cast material is heavily worked. This working and annealing procedure produces an equiaxed α microstructure from which conventional heat treatments are performed to obtain specific mechanical properties depending on the service application. AM Ti-6Al-4V, however, has a vastly different initial microstructure compared to its wrought counterpart. The equiaxed α microstructure for wrought material is replaced with a fine acicular α' (martensitic) microstructure for Ti-6Al-4V parts fabricated by the L-PBF process. This difference in initial microstructure results in conventional Ti-6Al-4V heat treatments having less of an effect on the microstructure and resulting mechanical properties.

Vrancken et al. [8] investigated the different response of L-PBF Ti-6Al-4V alloy on generally applied heat treatments and distinguished the influence of time, temperature, and cooling rate. They concluded that heat treating at intermediate to high temperature below β -transus, followed by furnace cooling, was optimal for the overall optimization of tensile properties. They also claimed that due to the specific process conditions and specific microstructure, application of standard heat treatments of the L-PBF-produced parts does not lead to the usual or expected results and needs to be treated differently than bulk alloy parts.

Vrancken et al. [8] and Sercombe et al. [17] performed optimization of mechanical properties of Ti-6Al-4V alloy via heat treatment of parts produced by the L-PBF below and above β -transus temperature. They found that through heat treatment of the L-PBF Ti-6Al-4V alloy below β -transus temperature made the β grain boundaries more visible; the

microstructure no longer contained long columnar prior β grains after heat treatment above the β -transus, indicating extensive grain growth, up to the point of semi-equiaxed β grains.

Facchini et al. [18] performed post-fabrication heat treatment (hot worked and annealed) of a L-PBF Ti-6Al-4V alloy causing the transformation of the metastable martensite to a biphasic α - β matrix resulting in an increase in ductility and a reduction in strength. Vilaro et al. [19] experimented and compared AF and both sub-transus and super-transus heat-treated (through solution treatment and tempering) L-PBF Ti-6Al-4V alloy processed by which exhibited high yield and ultimate strengths while the ductility was also significantly improved as compared to the AF sample. Fan et al. [20] examined the effects of process parameters of L-PBF (laser power, scanning speed, scanning direction) and heat treatment (through the solution and aging heat treatment) on the microstructure and properties of Ti-6Al-4V alloy forming parts under coaxial powder feeding and observed that the original properties can be improved and the high performance can be obtained. They concluded that solid solution and aging heat treatment are capable of improving the strength and plasticity of deposited Ti-6Al-4V alloy.

Galarraga et al. [21] studied the effect of different heat treatments on the microstructure of the EBM Ti-6Al-4V ELI (extra low interstitial) and its impact on the mechanical properties. They observed that faster cooling rates after solution heat treatment produced a greater amount of α' martensitic phase, with water quenching resulting in a fully α' microstructure. However, by increasing α lath thickness (from 0.62 to 2.9 μm), they observed a detrimental effect on mechanical properties like reducing microhardness, yield stress, ultimate tensile strength, and elongation to failure by 11%, 8.5%, 1.5%, and 26% respectively. Zhao et al. [22] investigated the effect of several heat treatments, both below and above β -transus temperature on the microstructure and microhardness of L-PBF Ti-6Al-4V alloy and found that the original martensitic α' phase converts into the α phase. After annealing below β -transus temperature, the α phase starts to dissolve into the β phase under equilibrium heating conditions forming a lamellar $\alpha + \beta$ mixture with lower hardness and greater ductility. However, at temperatures above β -transus, the microhardness increases significantly.

The Ti-6Al-4V alloy fabricated by the L-PBF method has been extensively studied for various heat treatments with the purpose of relieving stress and achieving an equilibrium microstructure, eliminating the metastable α' martensite phase and obtaining a microstructure with exclusively α and β phases. However, for the L-PBF process, the relation between microstructure and mechanical properties after heat treatment has been mainly limited to the AF condition and similar to other AM processes; it does not completely prevent the presence of porosity in the build.

The microstructure and properties of Ti-6Al-4V, as an $\alpha + \beta$ alloy which is capable of combining both the strength of α -phase alloys with the ductility of β -phase alloys, can be varied widely by appropriate heat treatments and thermo-mechanical processing [21]. Different variations of microstructures can be achieved with the application of different simple thermo-mechanical treatments at above and below β -transus on this $\alpha + \beta$ alloy. Therefore, it is crucial to study the effect of various heat treatments on microstructure and subsequent impacts on micromechanical properties of the AM $\alpha + \beta$ Ti-6Al-4V alloy to verify its performance in load-bearing applications.

Having said this, the current study aims to understand the effect of various heat treatments on the microstructure of the L-PBF Ti-6Al-4V and its impact on micromechanical properties obtained through an instrumented nanoindentation testing method. The heat treatments utilized in this work were designed through four various heat treatment cycles. The effect of post-heat treatment including solutionizing followed by water quenching (WQ), air cooling (AC), furnace cooling (FC), and aging (precipitation hardening, PH) on subsequent formation of different microstructural phases and their impact on micromechanical properties were investigated using a non-destructive instrumented nanoindentation approach. Microstructural quantitative analyses (i.e., optical microscopy (OM) and scanning electron microscopy (SEM)) were performed to assess the microstructure of heat-treated AM Ti-6Al-4V $\alpha + \beta$ alloy.

2 Experimental procedures

2.1 Sample preparation

The material utilized here to study various cooling rates of different heat treatment cycles is an additive manufactured Ti-6Al-4V alloy fabricated via the L-PBF process. The rectangular samples with dimensions of $9.8 \times 9.8 \times 5.6 \text{ mm}^3$ (5.6 mm height) were fabricated. In order to investigate the effect of various heat treatment cycles on microstructure and micromechanical properties of the printed materials, the samples were cut into half exactly at the middle from the bottom surface to the top. Four as-printed rectangular samples were thus prepared to study post-heat treatment effect with dimensions of $9.8 \times 4.9 \times 5.6 \text{ mm}^3$. The AM process parameters chosen to manufacture parts is summarized in Table 1. This set of parameters are the recommended performance parameters provided by the equipment manufacturer. It is worth mentioning that the process parameters can have significant effects on the resulting mechanical properties. However, this study is focused on the effect of various thermal treatment cycles on the micromechanical properties as evidenced by the nanoindentation testing. Though the optimization of the parameters

Table 1 Parameters used for the manufacturing of Ti-6Al-4V parts

System	EOS M290
Substrate material	Ti
Powder description	Gas atomized, air dried
Mean particle diameter	35 μm
Powder layer thickness	30 μm
Laser spot diameter	100 μm
Laser power	285 W
Scan speed	1200 mm/s
Shielding gas type	Argon
Shielding gas inlet temperature	20 $^{\circ}\text{C}$
Shielding gas inlet flow rate	0.25 m^3/s

is not the main focus of this paper, the main requirement would be that the initial conditions for all the samples were similar (i.e., similar process parameters were used for each specimen). The fact that all the specimens were fabricated using the same process conditions means any significant changes in the micromechanical properties can be related directly to the thermal treatments for each specimen.

2.2 Heat treatment procedures

Heat treatment of the samples was carried out in a KSL-1100X muffle furnace, a heating atmosphere-controlled muffle furnace for material synthesis under controlled inert gas atmosphere, with accuracy of $\pm 1 \text{ }^{\circ}\text{C}$. At first, the samples were solutionized through heating at $950 \text{ }^{\circ}\text{C}$ with a heating rate of $15.8 \text{ }^{\circ}\text{C}/\text{min}$ and then soaking at $950 \text{ }^{\circ}\text{C}$ for 1 h. Upon completion of the solution treatment, various cooling regimes including water quenching (WQ), air cooling (AC), and furnace cooling (FC) were executed on the printed samples (see Fig. 1). Air cooling was performed by cooling the sample in the air. Furnace cooling was carried out by turning off the heating. A separate sample was employed for aging (i.e., precipitation hardening) heat treatment purpose. This was done in

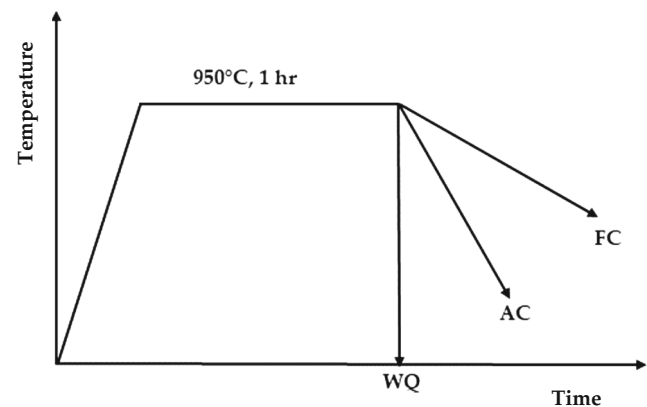


Fig. 1 Three different types of heat treatment: water quenching (WQ), air cooling (AC), and furnace cooling (FC)

order to reveal the effect of aging heat treatment on microstructure and micromechanical property evolution. To perform aging heat treatment, the sample was soaked at 950 °C for 1 h, then quenched and artificially aged. The aging cycle included heating at 540 °C for 5 h following by air cooling. The schematic of the aging heat treatment is shown in Fig. 2.

2.3 Instrumented indentation

The instrumented indentation testing technique (i.e., micro/nanoindentation), a continuous measurement of force (in the range of nN to mN) and displacement (in the range of nm to μm based on the depth sensitivity or average property required from the substrate), is considered a reliable, convenient, and non-destructive testing technique to examine the microstructure/local mechanical property correlation in metals at ambient (room) and elevated temperatures. Nano/micromechanical properties (hardness, indentation stress, creep, indentation strain rate sensitivity, reduced Young’s modulus, etc.) of the material could be measured from the load (*P*) and displacement (*h*) data recorded throughout the process in the form of load vs displacement (*P-h*) curve; see Fig. 3 [23, 24].

Micro- and nanohardness measurements were performed on the as-fabricated and the heat-treated samples using a Vickers hardness testing machine (HM 112 Mitutoyo) and a Hysitron Ubi-1 Nanoindenter, respectively. Nanoindentation tests were executed with a peak load of 10 mN and a loading rate of 2 mN/s using a self-similar pyramidal (Berkovich) indenter. Upon reaching to the maximum indenter load, the load was held constant for 5 s to let the indenter relax on the surface and then unloaded. Thermal drift corrections were ensured by the sample being unloaded to 10% of the peak and then holding for 120 s to ensure thermal drift is kept below 0.05 nm/s. Each indentation test was repeated 25 times to confirm reproducibility.

For the Vickers microhardness testing, a load of 0.5 kg f was employed with a dwell time of 12 s. Each plotted microhardness value is an average of three readings. For each

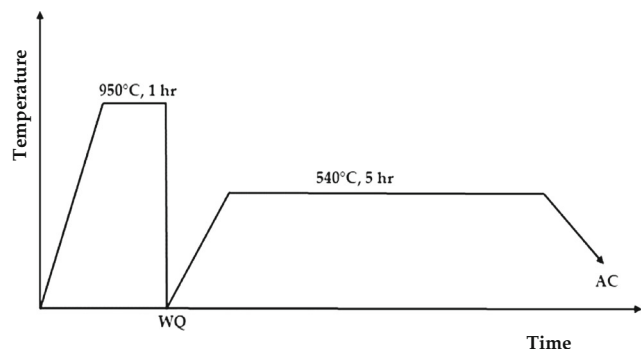


Fig. 2 Schematic of precipitation hardening heat treatment for the Ti-6Al-4V sample

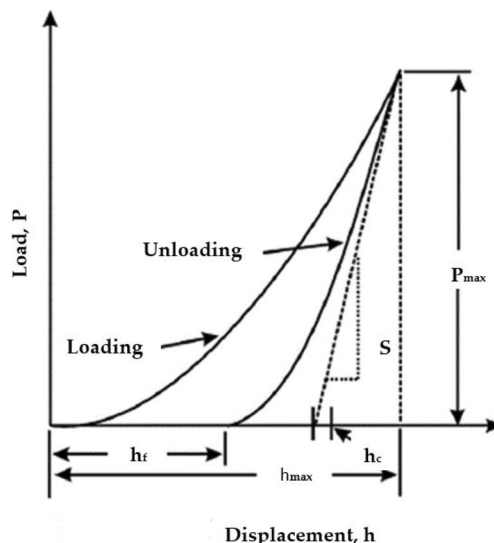


Fig. 3 Schematic representation of the *P-h* curve showing loading and unloading during nanoindentation [25]

sample, 25 positions were examined to confirm the reproducibility.

Before the indentation tests were performed, the surfaces of the samples were carefully ground with a series of progressively finer sandpapers followed by fine polishing which resulted in the mirror-like scratch-free surface finish. The microstructure was revealed upon using a modified Kroll’s reagent of 5 ml HF, 15 ml HNO₃, and 80 ml distilled water. The microstructure and grain sizes of the materials were then examined by optical microscopy (OM, MM500T) and scanning electron microscopy (SEM, QUANTA FEG 650).

The stress distribution pattern over various heat-treated samples obtained from the instrumented indentation testing supports the hardness variation obtained from the Vickers microhardness testing, confirming the reliability of this non-destructive testing technique. Indentation stress is calculated using the following equation [26, 27]:

$$\sigma_{ind} = \frac{P_{ind}}{24.56 \times C(h + 0.06R)^2} \tag{1}$$

Here, σ_{ind} is the indentation stress, *C* is the sink-in/pile-up factor, P_{ind} is the indentation load, *h* is the instantaneous contact depth, and *R* is the indenter tip radius due to blunting at the tip (which was 200 nm for the Berkovich indenter) used in this study.

The average indentation hardness (H_{ind}) can be written as

$$H_{ind} = \frac{P_{ind}}{A(h_c)} \tag{2}$$

Here, h_c is the instantaneous contact depth, and *A* is the indentation area.

The reduced modulus of elasticity, i.e., E_r , takes into account the final elastic constant of the diamond (Berkovich)

indenter and can be written as [28]

$$\frac{1}{E_r} = \frac{(1-\nu^2)}{E} + \frac{(1-\nu_i^2)}{E_i} \tag{3}$$

Here, E is the modulus of the specimen, E_i is the modulus of the indenter, ν is Poisson’s ratio of the specimen, and ν_i is Poisson’s ratio of the indenter.

The elastic recovery parameters (ERP) can be deduced from the following equation [28]:

$$ERP = \frac{h_{max} - h_c}{h_{max}} \tag{4}$$

Here, h_{max} is the maximum indentation depth and h_c is the contact depth (as shown in Fig. 3).

3 Results and discussion

3.1 Microstructure

Cooling rate, time, and temperature are the main parameters of heat treatment which affect the final microstructure of the Ti-6Al-4V alloy. In this study, the samples were solutionized at 950 °C for 1 h with the purpose of studying the effect of different cooling rates from below β -transus temperature on the resultant microstructure and micromechanical properties. Various cooling rates produce different microstructures as shown in the continuous cooling transformation curve (CCT diagram) in Fig. 4. This figure demonstrates different phase transformations of Ti-6Al-4V alloy in different temperature zones at various cooling rates. Fastest cooling method (WQ), intermediate cooling method (AC), and slowest cooling method (FC) significantly transform the phases of Ti-6Al-4V at both sub-transus and super-transus zones.

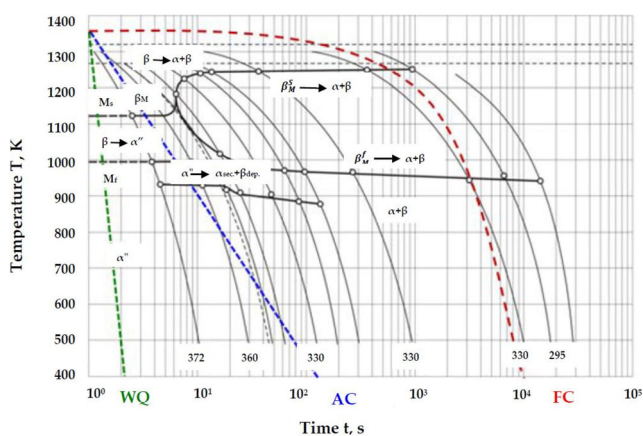


Fig. 4 CCT diagram for Ti-6Al-4V alloy showing cooling curves of three different cooling methods (water quenching, air cooling, and furnace cooling) [29]

Figures 5 and 6 show the optical and scanning electron microscopy images of the Ti-6Al-4V alloy in the AF and heat-treated conditions in X - Y direction. In the AF samples, the L-PBF is typically martensitic which does not allow for colonies to form. The acicular grain widths are controlled by the cooling rate, and the lengths are controlled by grain impingement (both β and α'). The colony size in martensitic Ti is taken to be the width of the α' needles. Additive manufactured α - β Ti-6Al-4V alloy is typically characterized with prior β grains that grow epitaxially through several layers, consisting of grain boundary α and martensitic α' [30–32]. The microstructure of the Ti-6Al-4V alloy can be typically described as primary α , secondary α , colony α , plate-like α , and martensite α' (α''), acicular α , grain boundary α , basket-weave structure [33], and Widmanstätten structure [34]. The terms basket-weave structure, Widmanstätten structure, and acicular are often used to be interchanged [45].

In the Ti-6Al-4V alloy manufactured by the L-PBF, an α - β lamellar structure associated with α -phase lamellae in a β -phase matrix is created due to the low to intermediate cooling rates experienced during the post-manufacture heat treatment processes. The α lamellae are created by diffusion-controlled nucleation and growth of α platelets into β grains [35]. In additively manufactured Ti-6Al-4V alloy, the size of these α platelets is controlled by the cooling rate of heat treatment processes; an increased cooling rate results in a decreased diffusion rate, which subsequently leads to decreased thickness of the α -lamellae associated with higher yield strength [36]. The length of α particles is controlled by grain impingement. The prior β grain size is typically determined by the amount of time the material is exposed to temperatures above β -transus, which is generally around 995 °C for the Ti-6Al-4V alloy [37].

Considering the cross-sectional microstructural morphology in Figs. 5 and 6, it is observed that the growth of the prior β grains is parallel to the scanning direction. It is further noticed that the columnar shape of the prior β grains is prolonged along the building direction, i.e., toward the substrate following the heat transfer direction. The columnar shape is formed by the epitaxial growth of the original β -phase due to successive layer deposition and the temperature gradient along the building direction of the L-PBF process.

It is quite possible to get an estimation of the mechanical properties of the material through microstructural characterization by a means of establishing the structure-property relationships. The α colony size is a microstructural feature that is known to affect mechanical properties significantly since it correlates with the slip lengths of the material [38]. Smaller α colonies contribute to higher strength, and their size correlates with α lath and grain boundary α thickness. Prior β grain boundary determines the size of the α colony. Faster cooling rate decreases the size of the α colonies along with the size of martensitic α' , α laths, and grain boundary α . From Figs. 5

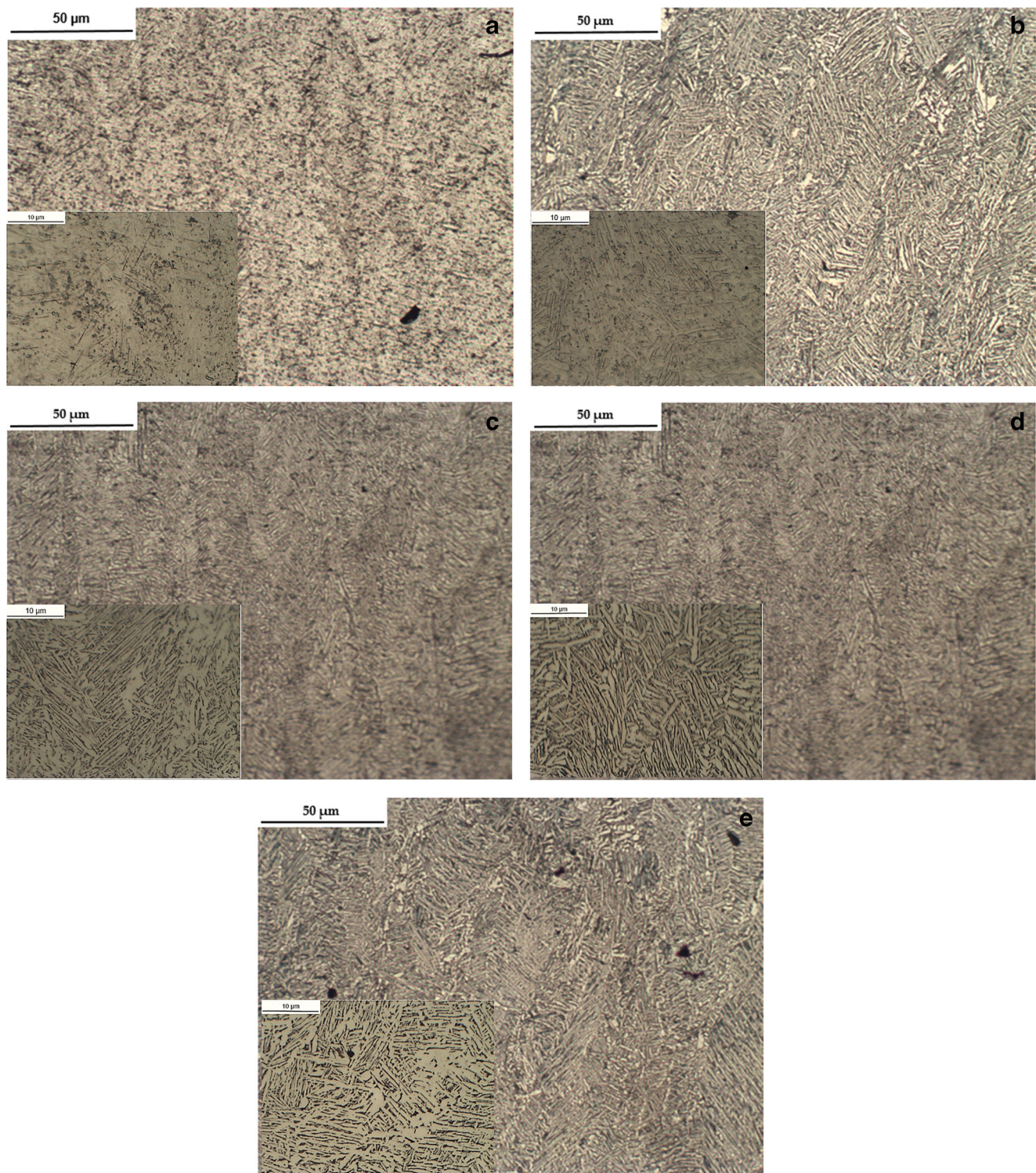


Fig. 5 Optical microscopy of **a** as-fabricated (AF), **b** air-cooled (AC), **c** furnace-cooled (FC), **d** water-quenched (WQ), and **e** aged (PH) microstructures

and **6**, it is observed that the size of the α colony is very fine in the PH sample rendering highest strength of all the heat-treated samples, followed by AC, FC, AF, and WQ samples.

Thijs et al. [7] observed the formation of intermetallic phase Ti_3Al precipitation at high heat input when the temperature reaches 500–600 °C. Due to rapid solidification during

the fabrication operation, segregation of Al leading to the precipitation of an intermetallic Ti_3Al phase occurs at grain boundaries. The solubility of Al is very low in Ti, and it causes solid solution strengthening along with precipitation strengthening [39]. Due to short interaction times coupled with a highly localized heat input, large thermal gradients exist during the

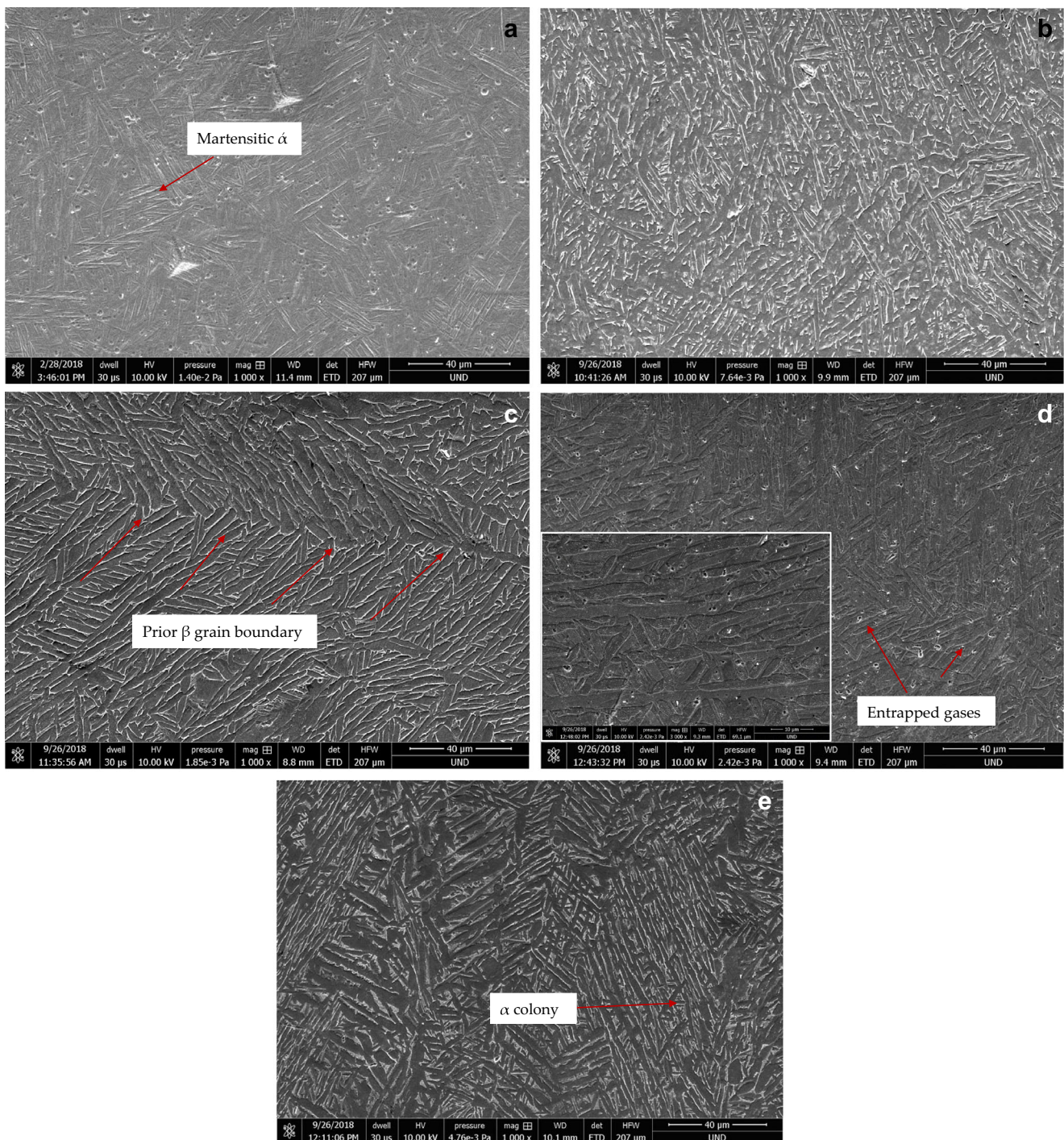


Fig. 6 SEM images of **a** as-fabricated (AF), **b** air-cooled (AC), **c** furnace-cooled (FC), **d** water-quenched (WQ), and **e** aged (PH) samples

process leading to the build-up of thermal stresses. Additionally, rapid solidification leads to segregation phenomena along with the development of a non-equilibrium process [8].

From Figs. 5 and 6, it appears that, after performing heat treating at 950 °C, primary α became significantly coarser which is similar to the observation of Vrancken et al. [8]. The WQ sample is the softest (which is confirmed after

performing the indentation on the samples based on the indentation depth and the obtained nanomechanical properties) one as this sample is solutionized and then water quenched. The expected state of the material is known as a supersaturated solid solution (SSSS). Upon holding for 1 h at 950 °C, various precipitates and strengthening phases are dissolved in the matrix and any segregation present in the alloy is reduced (see Figs. 5d and 6d). Upon quenching, the SSSS, which is in

equilibrium state, is formed. Here, the atoms do not have time to diffuse to potential nucleation sites and therefore the precipitation does not form. Heating the α - β Ti-6Al-4V alloy to the solution treatment (solutionizing) temperature produces a higher ratio of β -phase [8]. This partitioning of phases is maintained by quenching which results in a soft microstructure. Due to the rapid cooling rate, upon water quenching, it is assumed that martensitic α'' is developed in prior β grains.

Sub-transus heat treatment followed by air cooling and furnace cooling shows almost similar microstructure evolution. In AC samples, solutionizing at 950 °C strongly promoted grain growth, as clearly shown in Figs. 5(c) and 6(c). Due to a relatively higher cooling rate in comparison to the furnace cooling, the β phase is transformed into a finer lamellar structure in the AC sample. After intermediate cooling rates, i.e., when the samples were air cooled, a transformed β structure which is also known as bi-lamella structure started to appear in the AC samples formed by secondary α laths precipitated in the β matrix [38]. The heat treatment did not eliminate the microstructural anisotropy and was accompanied with α'' decomposition, lamella growth, and diffusion. The stable interwoven microstructure of the initial martensite severely hindered the grain growth.

In sub-transus heat treatment followed by furnace cooling, due to low to intermediate cooling rate, α -lamellae are created by diffusion-controlled nucleation and growth of α platelets into β grains [40]. During the subsequent heat treatment, the α' phase in the L-PBF-fabricated Ti-6Al-4V alloy is expected to slow down the growth of newly formed grains, leading to a fine $\alpha + \beta$ lamellar structure. After solutionizing, the α' phase was partially decomposed, while the prior α' phase is still clearly visible. As stated in Wu et al. [41], the decrement of dislocation density in the α phase and the decomposition of the α' phase are the two prime microstructural changes observed during the stress-relief heat treatment. Typically, an α colony is created from the β -single-phase field during slow cooling after an annealing treatment and the prior β grain size restricts the initial α colony size.

In the case of the L-PBF-fabricated Ti-6Al-4V alloy, during subsequent sub-transus treatment, the initial acicular martensite α' gradually decomposes into $\alpha + \beta$ in the shape of a colony containing parallel α lamellae. Vrancken et al. [8] had an almost similar observation. Vrancken et al. [8] observed that after heat treating for 2 h at 780 °C, followed by furnace cooling (FC), the fine martensitic structure has been transformed to a mixture of α and β , in which the α' phase is present as fine needles. After conducting heat treatment below the β -transus and at sufficiently low cooling rates, due to the formation of a layer of grain boundary α and the more aggressive etching of the $\alpha + \beta$ mixture as opposed to the original α' , the prior β grains became even more visible. However, the microstructure no longer contained long columnar prior β grains after treatment above the β -transus, indicating

extensive grain growth of the L-PBF material, up to the point of semi-equiaxed β grains. Studies by Sercombe et al. [17] and Vilaro et al. [19] have reported similar results regarding this microstructural transformation.

In the precipitation hardened (PH) sample, as shown in Figs. 5e and 6e, both α and β phases compete with each other to coarsen simultaneously but effectively hindered each other's growth, leading to a compact microstructure. Moreover, some nanosized particles are found to be dispersed on the α laths and α -phase grain boundaries of the air-cooled sample, as seen in Fig. 7, presenting some nanosized spherical particles on the surface of the AC sample and their numbers have significantly reduced in FC samples. There are currently limited reports of these nanosized particles generated in L-PBF Ti-6Al-4V alloy in the literature [42–44]. These nanosized particles are identified as the nanosized β particles [42]. The nanosized β particles also were observed in the spark plasma sintering fabricated Ti-6Al-4V alloy after aging at 450 °C [43]. Zhang et al. [44] through XRD analysis concluded that the nanosized particles are nanosized β particles in the α -phase matrix. In the current research, it was observed that the cooling rate influences this decomposition of nanosized particles, indicating these particles to be metastable and temperature sensitive. As showed in Fig. 7, during the FC, some of these nanosized particles dissolved into the α matrix, which is similar to the observation of Zhang et al. [44].

3.2 Microhardness

The Vickers microhardness evolution of the Ti-6Al-4V alloy produced by the L-PBF in as-fabricated and heat-treated conditions is presented in Fig. 8. The as-fabricated L-PBF Ti-6Al-4V sample consists of martensitic α' microstructure with an average hardness number of 359 HV_{0.5}. The microhardness values were increased for the AC and FC samples. The average microhardness values of 476 HV_{0.5}, with air cooling, and 390 HV_{0.5}, with furnace cooling, were measured. The microhardness of the WQ sample (SSSS) was found to be the lowest, with an average microhardness of 317 HV_{0.5}.

The average microhardness of the aged specimen (PH) was recorded as 528 HV_{0.5} which is the highest measured hardness in the current study. In the aging heat treatment, both α and β phases tended to coarsen simultaneously, while hindering each other's growth. This phenomenon led to a compact microstructure which resulted in an increase in microhardness. Yan et al. [45], after heat treating L-PBF Ti-6Al-4V alloy at 800 °C, 900 °C, and 1080 °C, found Vickers microhardness of 367 HV_{0.2}, 344 HV_{0.2}, and 421 HV_{0.2}, respectively, which are in agreement with the results obtained in this study. Furthermore, this variation in hardness is confirmed by the nanoindentation investigation of the AF and heat-treated samples.

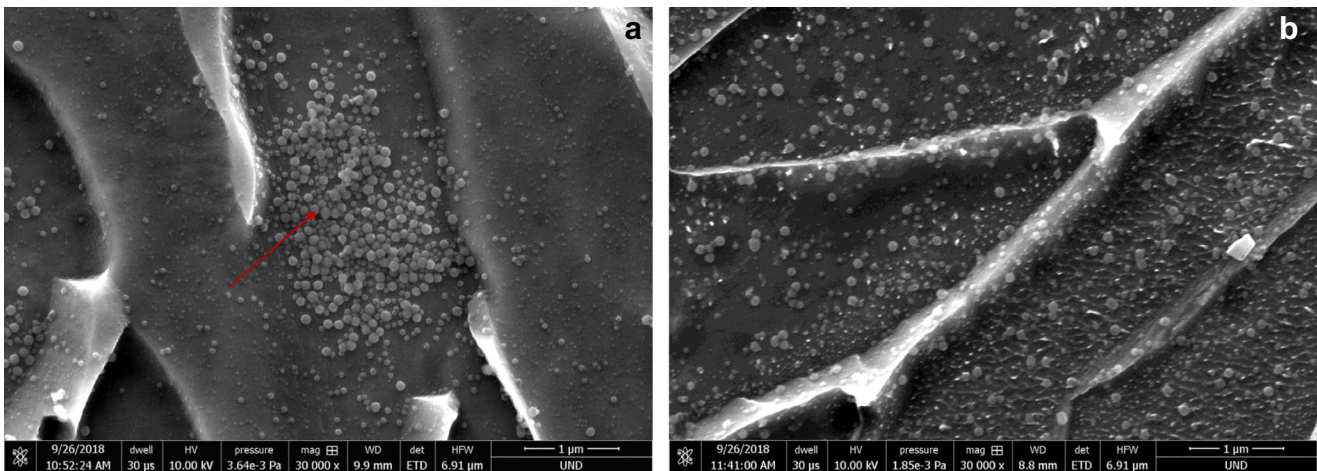


Fig. 7 a Nanosized particles in AC sample, b nanosized particles being dissolved in FC samples

3.3 Indentation responses

The load/displacement ($P-h$) curves with a loading rate of 2 mN/s and holding time of 5 s for AF and heat-treated samples at a peak load of 10 mN are shown in Fig. 9. Load plateaus are observed at constant load holding stage and its instantaneous displacement variation with different types of heat treatment. Indenter displacements within the specimen, h , for the PH, AC, FC, AF, and WQ samples are 121 nm, 148 nm, 189 nm, 223 nm, and 256 nm, respectively. The PH samples showed the least indentation depth, exhibiting the highest hardness of all the heat-treated samples. The PH sample consisted of mostly compact α growth along the prior β which develops in an epitaxial way, resulting in less penetration of the indenter. The indentation depth is followed by AC, FC, and WQ samples. The compact connected semi-equiaxed formation of α and martensitic α' in PH, AC, and FC samples is the reason behind their less indentation penetration depth as

compared with the AF sample. The less compact formation of α and α' in the WQ sample due to incompatibility to complete full transformation during cooling along with the presence of defects (i.e., entrapped gas pores) made the material soft which led to large indentation penetration depths.

Plasticity index is defined as the ratio of indentation hardness to the reduced modulus of elasticity [46]. Reduced modulus of elasticity represents the elastic deformation that occurs in both sample and indenter tip. Figure 10 shows the plasticity index of different heat-treated samples. H and E_r are calculated using Eqs. 2 and 3, respectively. Considering the H/E_r measured through the nanoindentation, the WQ sample possesses the lowest value. The hardness and elastic modulus are directly related to the cooling rates experienced in each employed heat treatment cycle. This fact is further supported by the elastic recovery parameters (ERP) of the heat-treated samples as shown in Fig. 11. The ERP of different heat-treated samples is determined using Eq. 4. ERP is a dimensionless index

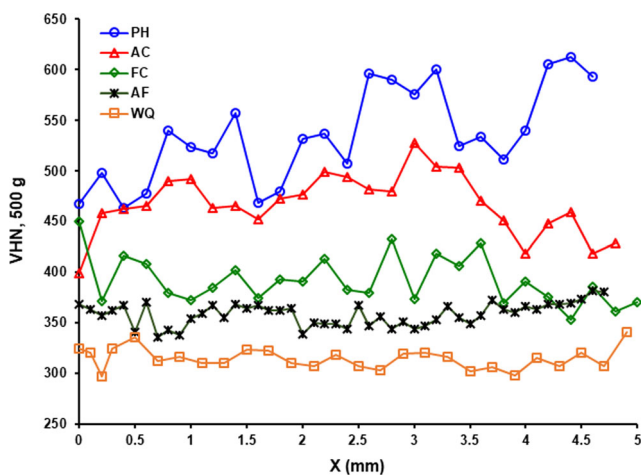


Fig. 8 Vickers microhardness of L-PBF Ti-6Al-4V alloy of as-fabricated and various heat-treated samples

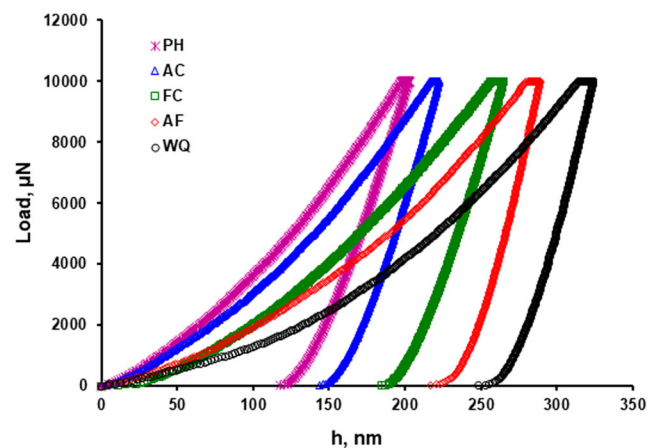


Fig. 9 $P-h$ curves demonstrating the indentation response of as-fabricated and various heat-treated samples

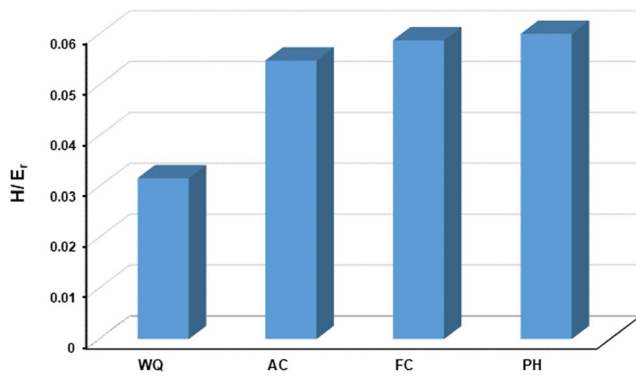


Fig. 10 Variation of the plasticity index across different heat-treated samples

which is closely related to the ratio between hardness and Young's modulus. ERP is lowest in the WQ sample, confirming it to have the softest microstructure.

3.4 Indentation size effect

Indentation size effect (ISE) is a well-known phenomenon where indentation hardness or indentation stress varies as a function of indentation depth or impression size [47–49]. The ISE is typically attributed to geometrically necessary dislocations (GNDs) by “mechanism-based gradient plasticity theory” in the plastic zone under the indents caused by strain, which are formed to sustain the imposed displacement for the sake of compatibility [5, 50–52]. Although the conventional plasticity predicts that the hardness should be independent of the indentation penetration depth, experimental findings, however, have shown that the hardness is a function of indentation depth, which is commonly termed as the ISE [53, 54]. The typical indentation size effect is reported to be an increase in hardness by decreasing the indentation depth.

After indenter penetration, the GNDs are generated in the material to accommodate the lattice rotation induced by the shape of the indenter. This nucleates extra dislocation in

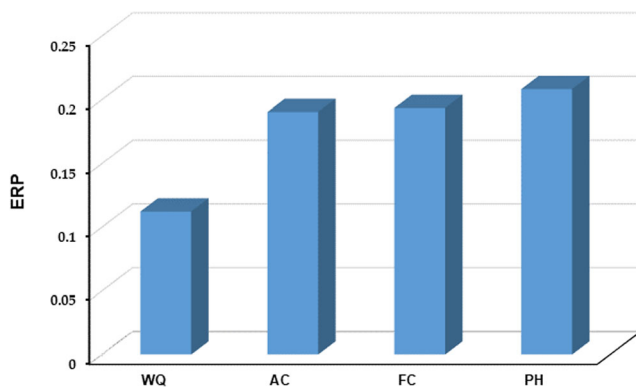


Fig. 11 Elastic recovery parameters (ERP) of the heat-treated samples

comparison to uniformly strained material in a very small region just below the indenter. Thus, GNDs may be positioned along non-easy slip crystals, resulting in fundamentally different Burger's vectors and mobility acting as barriers to ordinary dislocations. Large amounts of GNDs collectively lead to strain gradient or work hardening underneath the indenter. Higher indentation loading rate and density of GNDs cause the large strain gradients and work hardening effect which is more pronounced near the surface as compared with large depths.

Voyiadjis et al. [55] investigated indentation experiments on various single and polycrystalline materials and came to the conclusion that the indentation depth, temperature, and deformation rate all play vital roles in the strain gradient. Babu et al. examined nanomechanical behavior for traditionally built Ti-6Al-4V alloy, and strong indentation size effects were discovered with gradual decreases of nanohardness and Young's modulus with the increase of indentation depth [56]. Figure 12 demonstrates the indentation stress versus indentation displacement curve. Indentation stress was calculated by using Eq. 1. Strong indentation size effects are observed for the additively manufactured Ti-6Al-4V alloy in heat-treated conditions. From Fig. 12, it is observed that all the heat-treated samples experience a sharp decline of the indentation stress in shallower depth, which almost becomes constant at a larger depth, demonstrating a strong size effect for the heat-treated samples. As shown in the micrographs of the heat-treated samples, the PH sample contains the most compact growth of α , resulting in exhibiting the highest indentation stress of all the samples, followed by AC, FC, AF, and WQ samples.

In order to further assess the indentation size effect according to the Nix-Gao model [57], H_{ind}^2 was calculated using Eq. 2 and was plotted against $1/h$, according to $H_{ind}^2 = H_0(1 + h_0/h)$, as shown in Fig. 13 for different heat-treated samples. As seen, the characteristic linear dependence as predicted by Nix and Gao [57] is obtained for large

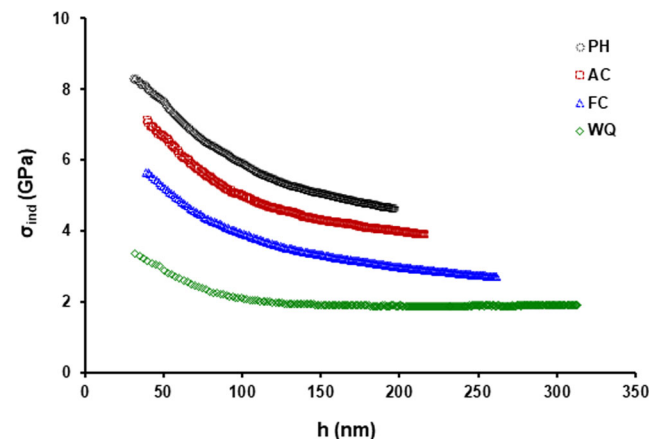


Fig. 12 Indentation size effect of various heat-treated samples

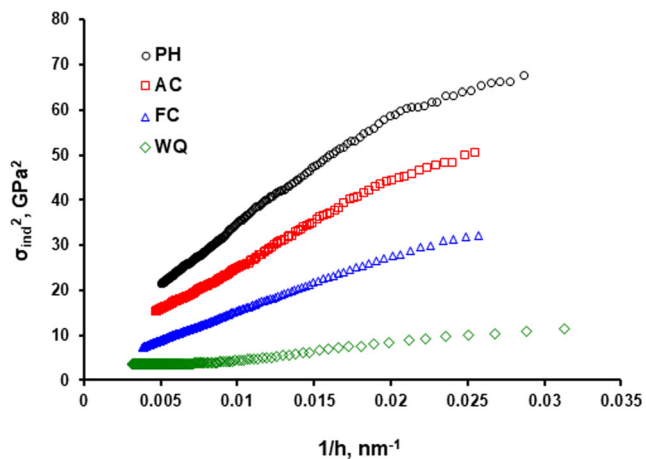


Fig. 13 Indentation size effect measured for different heat-treated samples

indentation depths, whereas for small depths, some measured deviation from the linear trend is observed.

4 Conclusions

The current research studied the effect of various heat treatment cycles on the microstructure of the L-PBF Ti-6Al-4V and its impact on micromechanical properties obtained through a non-destructive instrumented nanoindentation testing method. The hardness variation obtained from Vickers microhardness testing is in agreement with the stress distribution pattern over various heat-treated samples obtained from instrumented indentation, confirming the reliability of this non-destructive testing technique. The following conclusions have been drawn from the experimental observations and measurements:

- After heat treating at 950 °C, primary α became significantly coarser and connect with each other to form a compact structure.
- In the aging heat treatment, both the α and β tended to coarsen simultaneously, while effectively hindering each other's growth. This resulted in an aged sample having the highest microhardness of all the heat-treated samples, followed by air-cooled and furnace-cooled samples.
- The incompatibility to complete full transformation during cooling along with the presence of defects and entrapped gases causing the less compact formation of α and α' in the water-quenched sample led to the highest indentation penetration depth in this sample.
- A clear indentation size effect (ISE response) primarily attributed to the GNDs was observed in the indentation stress versus indentation depth graphs in heat-treated samples.

Funding information The authors greatly acknowledge funding provided by NDEPSCoR (Grant No.: 272531021). This work was also partially supported by the National Science Foundation under Grant #1657195.

References

1. Bian L, Thompson SM, Shamsaei N (2015) Mechanical properties and microstructural features of direct laser-deposited Ti-6Al-4V. *JOM*
2. Donoghue J (2016) Hybrid additive manufacture and deformation processing for large scale near-net shape manufacture of titanium aerospace components, Thesis, University of Manchester, p. 201
3. Shamsaei N, Yadollahi A, Bian L, Thompson SM (2015) An overview of direct laser deposition for additive manufacturing; part II: mechanical behavior, process parameter optimization and control. *Addit Manuf*
4. Bremen S, Meiners W, Diatlov A (2012) Selective laser melting. A manufacturing technology for the future? *Laser Tech J* 9:33–38
5. Pegues J, Roach M, Scott Williamson R, Shamsaei N (2018) Surface roughness effects on the fatigue strength of additively manufactured Ti-6Al-4V. *Int J Fatigue* 116:543–552
6. Murr LE et al (2009) Microstructure and mechanical behavior of Ti-6Al-4V produced by rapid-layer manufacturing, for biomedical applications. *J Mech Behav Biomed Mater*
7. Thijs L, Verhaeghe F, Craeghs T, Van Humbeeck J, Kruth JP (2010) A study of the microstructural evolution during selective laser melting of Ti-6Al-4V. *Acta Mater*
8. Vrancken B, Thijs L, Kruth J-P, Van Humbeeck J (2012) Heat treatment of Ti6Al4V produced by selective laser melting: microstructure and mechanical properties. *J Alloys Compd*
9. Seshacharyulu T, Medeiros SC, Morgan JT, Malas JC, Frazier WG, Prasad YVRK (2000) Hot deformation and microstructural damage mechanisms in extra-low interstitial (ELI) grade Ti-6Al-4V. *Mater Sci Eng A*
10. Naughton MD, Tiernan P (2007) Mechanical behaviour and superplastic forming capabilities of extra-low interstitial grade Ti-6Al-4V wire alloy with numerical verification. *Proc Inst Mech Eng Part L J Mater Des Appl*
11. Venkatesh BD, Chen DL, Bhole SD (2009) Effect of heat treatment on mechanical properties of Ti-6Al-4V ELI alloy. *Mater Sci Eng A*
12. Jovanović MT, Tadić S, Zec S, Mišković Z, Bobić I (2006) The effect of annealing temperatures and cooling rates on microstructure and mechanical properties of investment cast Ti-6Al-4V alloy. *Mater Des*
13. Donachie MJ (2000) Titanium – a technical guide, ASM Int. 2nd Ed
14. Zhang W, Wu B, Zhao WS, Li DX, Sui ML (2006) Formation of novel β -Ti martensites in Ti-6Al-4V under an electric-current-pulse heat treatment. *Mater Sci Eng A*
15. W. Callister and D. Rethwisch, *Materials science and engineering: an introduction*. 2007
16. Zhang B, Ham K, Shao S, Shamsaei N, Thompson SM (2017) Effect of heat treatment and hot isostatic pressing on the morphology and size of pores in additive manufactured Ti-6Al-4V parts. In: *Proceedings of the solid freeform fabrication*
17. T. Sercombe, N. Jones, R. Day, and A. Kop, Heat treatment of Ti-6Al-7Nb components produced by selective laser melting, *Rapid Prototyp. J.*, 2008
18. L. Facchini, E. Magalini, P. Robotti, A. Molinari, S. Höges, and K. Wissenbach, Ductility of a Ti-6Al-4V alloy produced by selective laser melting of prealloyed powders, *Rapid Prototyp. J.*, 2010
19. Vilaro T, Colin C, Bartout JD (2011) As-fabricated and heat-treated microstructures of the Ti-6Al-4V alloy processed by selective laser melting. *Metall. Mater. Trans A Phys Metall Mater Sci*

20. Z. Fan and H. Feng, Study on selective laser melting and heat treatment of Ti-6Al-4V alloy, *Results Phys.*, 2018
21. H. Galarraga, R. J. Warren, D. A. Lados, R. R. Dehoff, M. M. Kirka, and P. Nandwana, Effects of heat treatments on microstructure and properties of Ti-6Al-4V ELI alloy fabricated by electron beam melting (EBM), *Mater. Sci. Eng. A*, 2017
22. Zhao ZY et al (2018) The heat treatment influence on the microstructure and hardness of TC4 titanium alloy manufactured via selective laser melting. *Materials* (Basel)
23. Schuh CA (2006) Nanoindentation studies of materials. *Mater Today* 9(5):32–40
24. A. C. Fischer-Cripps, Nanoindentation, in *Nanoindentation*, 2011, pp. 21–38
25. N. Barbakadze, Local mechanical properties of the head articulation cuticle in the beetle *Pachnoda marginata* (Coleoptera, Scarabaeidae), *J Exp Biol.*, 2006
26. Poisl WH, Oliver WC, Fabes BD (1995) The relationship between indentation and uniaxial creep in amorphous selenium. *J Mater Res* 10(8):2024–2032
27. Lucas BN, Oliver WC (1999) Indentation power-law creep of high-purity indium. *Metall Mater Trans A* 30:601–610
28. M. Haghshenas and R. J. Klassen, Indentation-based assessment of the dependence of geometrically necessary dislocations upon depth and strain rate in FCC materials, *Mater Sci Eng A*, 2013
29. J. Sieniawski, W. Ziaja, K. Kubiak, M. Motyka, Titanium alloys-advances in properties control, 2013
30. Baufeld B, Van Der Biest O, Gault R (2009) Microstructure of Ti-6Al-4V specimens produced by shaped metal deposition. *Int J Mater Res* 100(11):1536–1542
31. de Formanoir C, Michotte S, Rigo O, Germain L, Godet S (2016) Electron beam melted Ti-6Al-4V: microstructure, texture and mechanical behavior of the as-built and heat-treated material. *Mater Sci Eng A* 652:105–119
32. Wang F, Williams S, Colegrove P, Antonysamy AA (2013) Microstructure and mechanical properties of wire and arc additive manufactured Ti-6Al-4V. *Metall Mater Trans A Phys Metall Mater Sci* 44(2):968–977
33. Ahmed T, Rack HJ (1998) Phase transformations during cooling in $\alpha+\beta$ titanium alloys. *Mater Sci Eng A*
34. Lütjering G, Williams JC (2007) Special properties and applications of titanium. In: *Titanium*
35. Haghshenas M, Totuk O, Masoomi M, Thompson SM, Shamsaei N (2017) Small-scale mechanical properties of additively manufactured Ti-6Al-4V. In: *Solid freeform fabrication symposium* Łukaszek-Sołek A, Krawczyk J (2013) Microstructure and phase transformation of Ti-6Al-4V. *Mater Sci Eng A* 2(1–2):27–30
37. M. Neikter, P. Åkerfeldt, R. Pederson, and M. L. Antti, Microstructure characterisation of Ti-6Al-4V from different additive manufacturing processes, in *IOP Conf Ser Mater Sci Eng*, 2017, vol. 258, no. 1
38. G. Lütjering, Influence of processing on microstructure and mechanical properties of ($\alpha+\beta$) titanium alloys, *Mater Sci Eng A*, 1998
39. R. Boyer, G. Welsch, E.W. Collings, *Materials properties handbook: titanium alloys*. 1994
40. Leuders S, Thöne M, Riemer A, Niendorf T, Tröster T, Richard HA, Maier HJ (2013) On the mechanical behaviour of titanium alloy TiAl6V4 manufactured by selective laser melting: fatigue resistance and crack growth performance. *Int J Fatigue* 48:300–307
41. S. Q. Wu, Y. J. Lu, Y. L. Gan, T. T. Huang, C. Q. Zhao, J. J. Lin, S. Guo, and J. X. Lin, Microstructural evolution and microhardness of a selective-laser-melted Ti-6Al-4V alloy after post heat treatments, *J Alloys Compd.*, 2016
42. Y. Xu, Y. Lu, K. L. Sundberg, J. Liang, and R. D. Sisson, Effect of annealing treatments on the microstructure, mechanical properties and corrosion behavior of direct metal laser sintered Ti-6Al-4V, *J Mater Eng Perform.*, 2017
43. Y. S. Zhang, J. J. Hu, Y. Q. Zhao, X. F. Bai, W. T. Huo, W. Zhang, and L. C. Zhang, Microstructure and mechanical properties of a high-oxygen core-shell network structured Ti6Al4V alloy, *Vacuum*, 2018
44. M. Zhang, Y. Yang, D. Wang, Z. Xiao, C. Song, and C. Weng, Effect of heat treatment on the microstructure and mechanical properties of Ti6Al4V gradient structures manufactured by selective laser melting, *Mater Sci Eng. A*, 2018
45. Yan X, Yin S, Chen C, Huang C, Bolot R, Lupoi R, Kuang M, Ma W, Coddet C, Liao H, Liu M (2018) Effect of heat treatment on the phase transformation and mechanical properties of Ti6Al4V fabricated by selective laser melting. *J Alloys compd* 764:1056–1071
46. Haghshenas M (2017) Multi-cycling instrumented nanoindentation of a Ti-23Nb-0.7Ta-2Zr-1.2O alloy in annealed condition. *Mater Sci Eng A*
47. Ando S, Nakamura K, Takashima K, Tonda H (1992) {1122} <1123> slip in magnesium single crystal, *Japan. Inst Light Met* 42(12):765–771
48. Haghshenas M, Wang Y, Cheng YT, Gupta M (2018) Indentation-based rate-dependent plastic deformation of polycrystalline pure magnesium. *Mater Sci Eng A* 716(November 2017):63–71
49. Stelmashenko NA, Walls MG, Brown LM, Milman YV (1993) Microindentations on W and Mo oriented single crystals: an STM study. *Acta Metall Mater* 41(10):2855–2865
50. Ma Q, Clarke DR (1995) Size dependent hardness of silver single crystals. *J Mater Res* 10(4):853–863
51. Ashby MF (1970) The deformation of plastically non-homogeneous materials. *Philos Mag* 21(170):399–424
52. Fleck NA, Muller GM, Ashby MF, Hutchinson JW (1994) Strain gradient plasticity: theory and experiment. *Acta Metall Mater* 42(2):475–487
53. Kiener D, Durst K, Rester M, Minor AM (2009) Revealing deformation mechanisms with nanoindentation. *JOM*
54. Pharr GM, Herbert EG, Gao Y (2010) The indentation size effect: a critical examination of experimental observations and mechanistic interpretations. *Annu. Rev. Mater. Res*
55. Voyiadjis GZ, Faghihi D (2012) Microstructure to macro-scale using gradient plasticity with temperature and rate dependent length scale. *Procedia IUTAM* 3:205–227
56. SridharBabu B, Kumaraswamy A, AnjaneyaPrasad B (2014) Effect of indentation size and strain rate on nanomechanical behavior of Ti-6Al-4V alloy. *Trans Indian Inst Metals* 68(1):143–150
57. Nix WD, Gao H (1998) Indentation size effects in crystalline materials: a law for strain gradient plasticity. *J Mech Phys Solids* 46:411–425

Publisher's note Springer Nature remains neutral with regard to jurisdictional claims in published maps and institutional affiliations.